Mass Transfer of Water Vapor in a Hollow Fiber for Degassing Processes

Hideyuki Murata, Yasushi Tomita, Makoto Miyashita, and Kazunari Sakai
Central Research Laboratories, Dainippon Ink & Chemicals, Inc., Chiba 285-0078, Japan

Masayuki Toda
Dept. of Material Science and Engineering, Yamagata University, Yamagata 992-0038, Japan

Tadahiro Ohmi
Dept. of Electronics, Tohoku University, Miyagi 980-0845, Japan

The mass-transfer mechanisms of water vapor in hollow-fiber membrane modules used to remove gases from water were studied experimentally and theoretically. Hollow-fiber modules for degassing are widely used in various industries, including ultrapure water production. Although these modules perform extremely well, a general principle for the design has not been established. Recently, very highly efficient asymmetric hollow-fiber modules were developed, that could reduce the dissolved oxygen to less than 1 μg/L (1 ppb). From our studies of the modules, it was found that the mass transfer of water vapor plays an extremely important role in the flow in the lumen side of the hollow fibers. The establishment of a theoretical design method for degassing modules can be expected from our studies.

Introduction

Recently, very high-quality ultrapure water was desired for washing semiconductors. To produce the ultrapure water, the removal of particles and fungus bodies in the water is essential. Even the removal of oxygen dissolved in the water is important, because the surface of semiconductors is oxidized by this dissolved oxygen.

Hollow-fiber membrane modules have been used recently to remove the oxygen because they have better performance than other conventional degassing equipment. There are two types of modules: one is the internal-flow module in which treated water flows in the lumen side of the hollow fibers, and the other is the external-flow type in which water flows in the shell side of the module. As for the methods of degassing, vacuum degassing or a nitrogen-purging method is used.

Recently, highly efficient external-flow modules comprising asymmetric hollow fibers were developed, which could reduce the dissolved oxygen to less than 1μg/L (1 ppb). For these modules, vacuum degassing is used mainly because of the ease of use.

Currently, larger modules are required for processing the huge amount of water in industrial-level operations. However, the enlargement of the module causes an increase in the length of the hollow fibers. Here, in order to design the modules it is important to understand the flows in the lumen side of the fibers. Because the permeation gases flow at a comparatively fast speed through the narrow lumen, pressure and velocity profiles are formed in the direction of the flows.

From our study, it was found that the volume of water vapor permeating through the membrane is more than that of dissolved oxygen and nitrogen. Therefore, the flow in the lumen is controlled by water vapor, so that the vapor dominates the pressure and velocity profiles. Consequently, understanding the mechanisms of water vapor permeation in a hollow-fiber membrane is extremely important for designing the degassing modules.

The mass transfer of oxygen in degassing modules has been extensively studied (Yang and Cussler, 1986; Li et al., 1995; Bessarabov et al., 1996), because the most important point

Correspondence concerning this article should be addressed to H. Murata.

for designing the modules is oxygen transfer in the liquid film adjacent to the membrane, which was pointed out in an earlier study (Yang and Cussler, 1986). Therefore, analysis of water flows (Lemanski and Lipscomb, 1995) is important, and improvement of the flow contributes to the design of high-performance degassing modules (Wang and Cussler, 1993). On the other hand, little attention has been paid to the flows in the lumen, which are mainly composed of water vapor, except for a few studies (Federspiel et al., 1996).

In this article, as the first step in establishing a design strategy for external-flow modules in vacuum degassing, we discuss the pressure and velocity profiles of water vapor in the lumen of hollow fibers from the viewpoint of mass transfer of the vapor, experimentally and theoretically. First, the transfer rates of water vapor were measured experimentally, and second, the pressure and velocity profiles, which were formed by the flow of water vapor in the lumen, were calculated analytically. As a consequence, it was found that pressure and velocity profiles in the lumen should be taken into account for designing the external-flow modules.

Vacuum Degassing Experiments

Material

The hollow fibers used here were asymmetric hydrophobic poly-4-methylpenten-1 of 255 μm OD and 35 μm wall thickness. The modules made from the fibers were cylindrical, and two types were used in this study. The first type was an external-flow module whose effective membrane area was 39.5 m^2, based on the outer membrane surface, and whose diameter and length were 18 cm and 68 cm, respectively. The second was an internal-flow module whose effective membrane area was 30.0 m^2, based on the inner membrane surface, and whose diameter and length were 16 cm and 57 cm, respectively.

In the operation of the external-flow module, treated water flows in the shell side of the module and permeated gases flow through the lumen side, while the opposite operations are conducted for the internal-flow module.

Method

Figure 1 shows the experimental setup. Water was circulated through the closed system, which consisted of a tank, a module, a pump, a heat exchanger, and pipes. The temperature of the water was maintained by the heat exchanger within an error of ± 0.2°C. The vacuum pump was used for degassing, and in some experiments, nitrogen sweep gas was used instead of the vacuum. The pumping speed of the vacuum pump mainly used in this study was 400 L/min. Regarding this vacuum pump, both a smaller and a larger one were used; their pumping speeds were 260 L/min and 3300 L/min, respectively.

When the degassing operation was started, the quantity of water inside the closed system decreased with time, because of water vapor permeation through the membranes. The decrease in the quantity of water was determined by tracing the level of decrease in the cylinder attached to the tank over a period of time. The operation pressure of the vacuum degassing was controlled by changing the length of the pipe between the module and the vacuum pump.

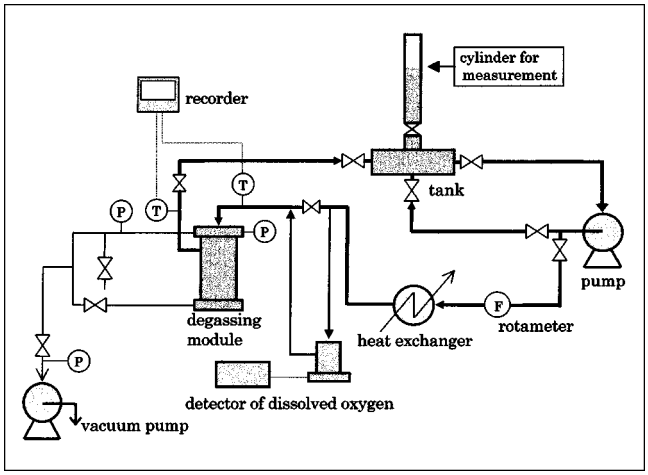

Figure 1. Experimental apparatus.

Results

Figure 2 shows the experimental results of the transfer rate of water vapor for vacuum degassing in the external-flow module. In this figure, the transfer rates of water vapor are plotted vs. the operation pressure. The pressure was manipulated by changing the length of the vacuum line; the operation temperatures were in the range of 15°C to 35°C within an error of ± 0.2°C.

The flow rates of the treated water were maintained at 1,000 L/h, where we confirmed that the transfer rates of water vapor were independent of the flow rates through the same experiments at 200 L/h and 500 L/h. These results show no mass-transfer resistance of water vapor in the liquid phase, which means that the water-vapor resistance exists in the membrane and the gas phase.

Generally, diffusivity in the membrane, which is hydrophobic, is much smaller than that in the gas phase. Thus, the

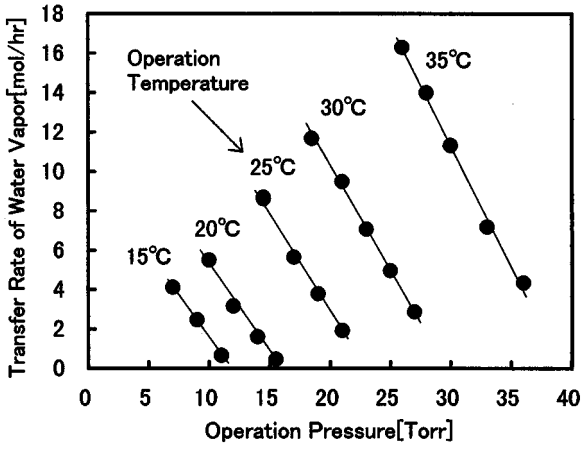

Figure 2. Transfer rate of water vapor in external-flow module.

Module type: external-flow module; membrane area: 39.5 m^2; water flow rate: 1000 L/h.

Table 1. Saturated Water-Vapor Pressure

Temp. [°C]	Pres. [torr]
15.0	12.79
20.0	17.54
25.0	23.76
30.0	31.83
35.0	42.18

transfer rate of water vapor is controlled by the mass transfer in the membrane.

As shown in this figure, the transfer rates of water vapor decrease as the operation pressure increases. These results indicate that the driving force of water vapor transfer is the pressure drop, which is the difference between the liquid–membrane surface and the gas–membrane surface in the membrane. The pressure of the liquid–membrane surface is the saturated water-vapor pressure, because the part of the membrane that is adjacent to the liquid phase is supposed to be filled with water vapor. The driving force therefore decreases with operation pressure and temperature increase because of its dependence on the saturated water vapor pressure (the saturated water vapor pressures are shown in Table 1). Thus, the transfer mechanism of water vapor can be described as follows:

$$\text{Transfer rate of water vapor} = QA\Delta p = QA(p_s - p), \quad (1)$$

where Q is the permeance of water vapor; A and Δp are the total membrane area and the pressure drop, respectively; and p_s and p are saturated water vapor pressure and operation pressure, respectively.

To calculate the permeance of water vapor from these results, see the transfer rates plotted vs. the pressure drop in Figure 3. Generally, the permeance is obtained as the slope from this kind of figure.

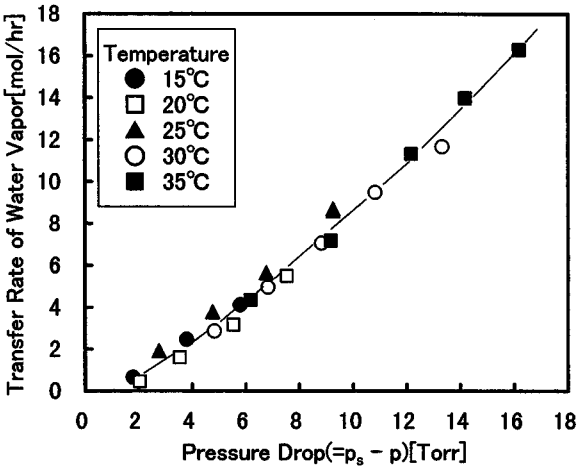

Figure 3. Transfer rate of water vapor vs. pressure drop in external-flow module.

Module type: external-flow module; membrane area: 39.5 m^2; water flow rate: 1000 L/h.

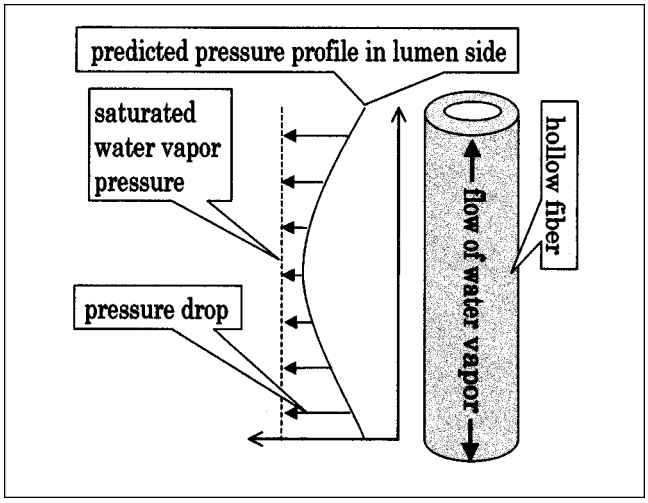

Figure 4. Pressure profile of water vapor in an external-flow module.

As shown in this figure, a nearly linear relationship was obtained, but contrary to the prediction shown in Eq. 1, the line does not reach the origin. Thus, the mechanism of the water vapor transfer must be reconsidered.

Here we focused on the lumen side of the hollow fibers as follows. The water vapor permeating through the membrane flows through the very narrow lumen (185 μm ID) at a comparatively high speed. Consequently, a pressure profile is formed in the direction of the flow. The operation pressure measured by a mercury manometer is therefore the value at the fiber end only, and the pressure at the other points in the lumen is not known.

From the preceding discussion, we determined that, because of the uncertainty of the pressure in the lumen, the permeance of water vapor could not be obtained from the experimental data of external-flow modules. To examine this assumption, the transfer rates of water vapor in the internal-flow module were measured, because the pressure is supposed to be uniform over the gas phase in the shell side and equivalent to the operation pressure.

Figures 4 and 5 illustrate, respectively, the predicted pressure profiles of an external- and an internal-flow module. Figure 4 illustrates the pressure profile of water vapor in the external-flow module, in which the pressure drop is supposed to decrease because of the fast flow along the fiber as the distance from one fiber end increases.

On the other hand, Figure 5 shows that the pressure of water vapor in an internal-flow module is uniform because the vapor flows outside (across) of the fibers (the shell side of the module); that is, across, not along the fibers. The pressure in the shell is also equivalent to the operation pressure for internal-flow modules. Therefore, the permeance can be obtained from the experimental data for the transfer rate of water vapor in the internal-flow module.

Figure 6 shows the results of the transfer rate of water vapor in an internal-flow module, in which the transfer rate was plotted vs. the pressure drop $(= p_s - p)$. The experiments were conducted at a constant flow rate of 1000 L/h

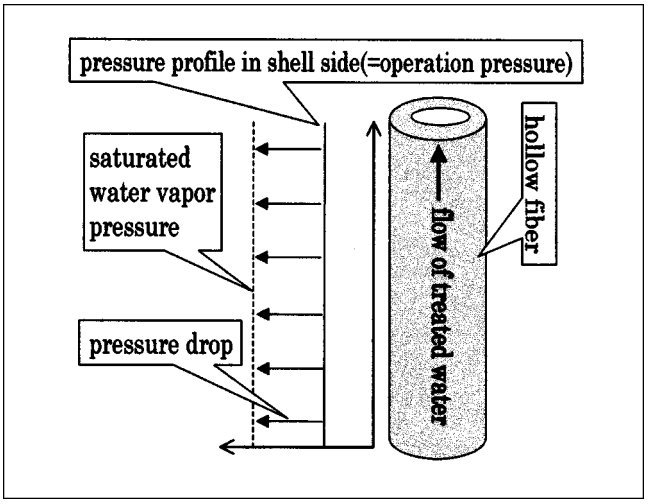

Figure 5. Pressure profile of water vapor in an internal-flow module.

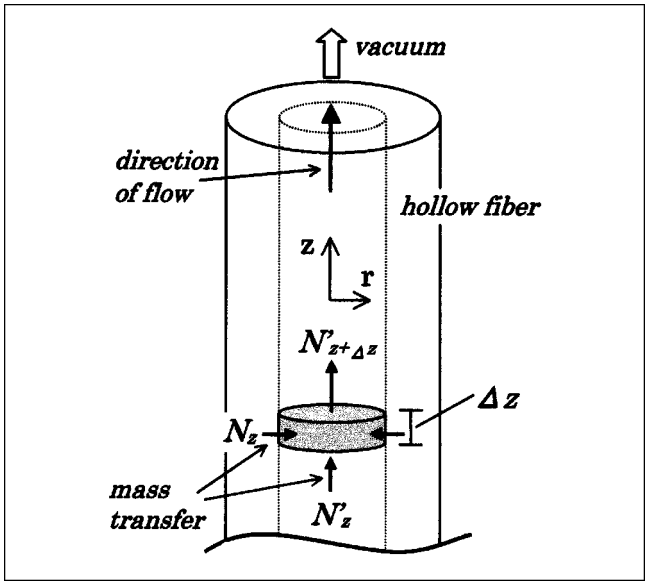

Figure 7. Hollow fiber used for theoretical analysis.

(the flow rate of treated water), within the 15–35°C range, which were the same conditions as in the previous experiments with an external-flow module.

As shown in Figure 6, the linear relationship (its slope is 1.526, the intercept is 0, and the correlation coefficient is 0.99) was obtained from the transfer rates of water vapor plotted vs. the pressure drops. Based on the results, the previous assumption (indicated in Eq. 1 and Figures 4 and 5) proved to be appropriate. Therefore, the permeance indicated in Figure 6 could be calculated from the slope of the solid line and the inner membrane area. The permeance obtained here must be used for external-flow modules because the value is unique to the membrane.

On the basis of the above experiments, the theoretical model for the analysis of the pressure profiles was developed below.

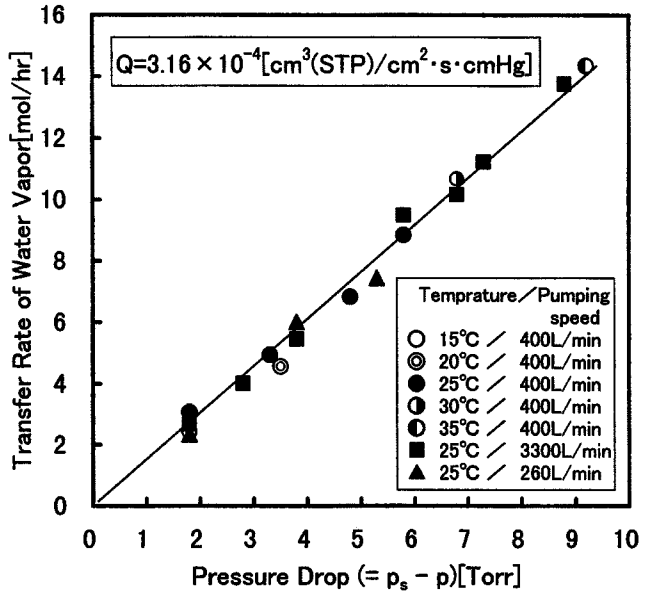

Figure 6. Transfer rate of water vapor vs. pressure drop in internal-flow module.

Module type: internal-flow module; membrane area: 30.0 m^2; water flow rate: 1000 L/h. *Q* was calculated on the basis of inner membrane area.

Theoretical Model for Vacuum Degassing

The analysis presented here is for calculating the pressure and velocity profiles of water vapor in the lumen of an external-flow module. Therefore, this analysis corresponds to the preceding experiments for the external-flow module. Only the transport of water vapor is considered; those of oxygen and nitrogen are neglected.

First, a mass balance and an equation of motion for water vapor in the lumen are required. Here, in calculating these governing equations, the following assumptions were made for the analysis

1. Ideal gas law is valid in the lumen.
2. End effects of hollow fibers are negligible.
3. Transport process is isothermal.
4. Axial diffusion is insignificant compared to the flow.

Figure 7 shows a hollow fiber for the theoretical model. Here, from the mass balance in the small cylinder, the governing equation describing the change in the flux of water vapor in the lumen is written as

$$\pi R_{\text{in}}^2 N_z' + 2\pi R_{\text{in}} \Delta z N_z = \pi R_{\text{in}}^2 N_{z+\Delta z}', \qquad (2)$$

where R_{in} is the inside radius of the hollow fiber; N_z is the permeation flux of water vapor; N_z' is the axial flux of water vapor; and Δz is the differential length of the hollow fiber.

The following differential equation is obtained by rewriting Eq. 2:

$$\frac{dN_z'}{dz} = \frac{2N_z}{R_{in}}. \quad (3)$$

The permeation flux, N_z, which is the flux through the membrane, is given by

$$N_z = Q(p_l - p) = Q(p_s - p), \quad (4)$$

where p_l is the water-vapor pressure at the liquid–membrane surface, which is equivalent to the saturated water-vapor pressure.

The axial flux N_z' can be expressed as

$$N_z' = -D\frac{dc}{dz} + c\bar{u} \cong c\bar{u} = \frac{p}{RT}\bar{u}, \quad (5)$$

where D and c are the diffusivity in the membrane and the concentration of water vapor, respectively, and $\bar{u}$ and p are the average axial velocity and the pressure in the lumen, respectively. Here in Eq. 5, the diffusion term is much smaller than the convection term of the bulk flow, so the first term on the right side is negligible.

Combining Eqs. 4 and 5 yields the following equation:

$$\frac{d}{dz}\left(\frac{p}{RT}\bar{u}\right) = Q(p_s - p) \quad (6)$$

This equation can be rewritten as

$$p\frac{d\bar{u}}{dz} + \bar{u}\frac{dp}{dz} = \frac{2RTQ}{R_{in}}(p_s - p). \quad (7)$$

Next, for the analysis of the flow in the lumen, the Reynolds number is calculated:

$$Re = \frac{\rho\bar{u}l}{\mu} = \frac{(pM_w/RT)ul}{\mu}$$
$$= \frac{\left({}^{20\times 133.3\times 0.018}/_{8.314\times 298.2}\right)\times 185\times 10^{-6}\times 0.5}{9.95\times 10^{-6}} < 1, \quad (8)$$

where Re is the Reynolds number; ρ and μ are the density and the viscosity of water vapor, respectively; and M_w is the molecular weight of water vapor. The typical pressure and velocity are, respectively, $p = 20$ torr and $\bar{u} = 0.5$ m/s, which were obtained through the preceding experiments with an external-flow module.

The viscosity of water vapor can be calculated through the following Chapman–Enskog's equation.

$$\mu[\mu\text{Pa}\cdot\text{s}] = 2.669\frac{(M_r T)^{0.5}}{\sigma^2\Omega_v}. \quad (9)$$

The calculated Re number indicates that the flow in the lumen is a viscous flow. Therefore, the velocity can be written in the following well-known form:

$$u(r) = -\frac{R_{in}^2}{4\mu}\frac{dp}{dz}\left\{1-\left(\frac{r}{R_{in}}\right)^2\right\} = 2\bar{u}\left\{1-\left(\frac{r}{R_{in}}\right)^2\right\}. \quad (10)$$

The following relationship can be obtained from this equation:

$$\frac{dp}{dz} = -\frac{8\mu}{R_{in}^2}\bar{u}, \quad (11)$$

where r is the radius coordinate.

Equations 7 and 11 are the governing equations for the water-vapor flow in the lumen. These equations can be solved simultaneously under the following initial conditions.

Initial Conditions (at one fiber end)

$p(0)$: operation pressure shown in Figure 2

$\bar{u}(0)$: calculated through the following relationship using transfer rate of water vapor, which corresponds to the $p(0)$ in Figure 2.

$$\text{Transfer rate of water vapor} = 2\times\pi R_{in}^2\bar{u}(0)\times\rho(0)\times m/M_w$$
$$= 2\times\pi R_{in}^2\bar{u}(0)\times\frac{p(0)}{RT}\times m, \quad (12)$$

where m is the total number of hollow fibers; and $\bar{u}(0)$, $\rho(0)$, and $p(0)$ are the values at one fiber end for the average velocity, density, and pressure, respectively.

The Runge–Kutta–Gill method was used for calculations using the preceding governing differential equations.

The permeance, Q, came from the experimental results for the internal-flow module indicated in Figure 6. Because Q is a value peculiar to the membrane, it can be applicable not only for internal-flow modules but also for external-flow modules. Therefore, the pressure and velocity profiles in the lumen can be obtained through this analysis.

Results of Analysis

Figure 8 shows the analytical solutions of the pressure and velocity profiles in the lumen when the operation temperature is 25°C and the operation pressure is 14.5 torr. The pressure and the velocity are plotted against the distance from one fiber end.

As shown in the figure, the pressure increases as the distance increases, while the velocity decreases and finally reaches zero. These results imply that no flow exists at distances of about 15.0 cm and greater. These may be unrealistic, however, because, at the point that the water vapor stops flowing, the pressure must be equivalent to the saturated water-vapor pressure. Thus, the proposed theoretical model has to be modified for establishment of a more accurate analysis.

As shown below, we conducted other experiments and analyses, and we reconsidered the theoretical model given earlier. As a result, a more precise modified model was obtained, which is discussed later (see the subsection on modified theoretical analysis).

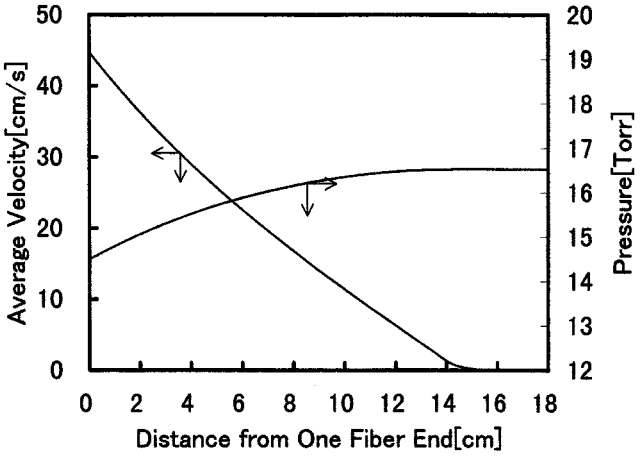

Figure 8. Calculated pressure and velocity profiles in the lumen.

Conditions for calculation: temperature: 25°C; pressure at one fiber end: 14.5 torr; transfer rate of water vapor: 8.7 mol/h.

Experiments and theoretical analysis for the nitrogen-purging method

From the preceding analytical results for vacuum degassing, it was found that the proposed theoretical model might not be accurate. It is very difficult to confirm the accuracy of the model, however, because both pressure and velocity are functions of the distance for vacuum degassing.

Thus, for a more detailed analysis, we used the nitrogen-purging method to conduct other experiments on the external-flow module, under the same conditions as in the previously cited experiments (flow rate of treated water, 1,000 L/h; temperature range, 15–35°C). We did this because, in the nitrogen-purging method, the velocity should be constant through the lumen because of the constant flow rate of the sweeping gas. Therefore, analysis using this method must be easier than that with vacuum degassing.

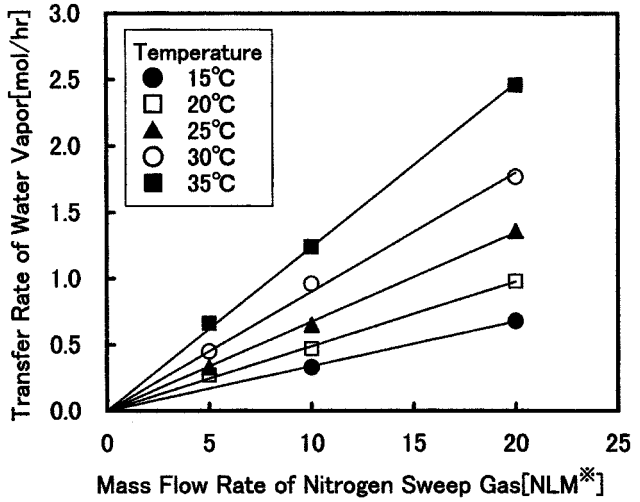

Figure 9. Transfer rate of water vapor with nitrogen-purging method.

Module type: external-flow module; membrane area: 39.5 m^2; water flow rate: 1,000 L/h. ※ NLM = normal liter per minute.

Figure 9 shows the experimental results in which the transfer rate of water vapor is plotted against the flow rate of nitrogen. Here nitrogen sweep gas was used to replace the vacuum pump. As shown in this figure, the transfer rate of water vapor increases as the flow rate of nitrogen and the temperature increase.

To understand the transport of water vapor in the nitrogen-purging method, theoretical analysis is required. The total pressure, p_t, is constant and equivalent to the atmospheric pressure. The p_t is given by

$$p_t = p + p_{N_2}, \tag{13}$$

where p_{N_2} is the partial pressure of nitrogen.

The governing mass balance can be described by the same form as in Eq. 2, and the permeation flux and the axial flux are given by Eqs. 4 and 5, respectively.

Combining Eqs. 2, 4, 5, and 13 yields the following differential equation:

$$\frac{dp}{dz} = \frac{2RTQ}{\bar{u}R_{\text{in}}}(p_s - p), \tag{14}$$

where $\bar{u}$ is assumed to be constant because of the constant flow rate of the nitrogen and the much smaller amount of permeated water vapor compared to the nitrogen flow.

The integration mentioned previously can be carried out easily, and the following equation for the permeance can be obtained:

$$Q = \frac{\bar{u}R_{\text{in}}}{2RTL} \ln \frac{p_s}{p_s - p_{\text{out}}}, \tag{15}$$

where L is the length of the hollow fiber, and p_{out} is the partial pressure of water vapor at the outlet (water vapor pressure at the downstream end of the fiber), which can be calculated from $p_{\text{out}}/p_{\text{atmosphere}}$ = transfer rate of water vapor/(transfer rate of water vapor + mass flow rate of nitrogen); $p_{\text{atmosphere}}$ denotes the atmospheric pressure.

The pressure profiles can be calculated from the following equation:

$$p = p_s\left\{1 - \exp\left(\frac{2RTQ}{\bar{u}R_{\text{in}}}z\right)\right\}. \tag{16}$$

The analytical results that were calculated from Eq. 15 are shown in Figure 10. Here, the permeance of water vapor is plotted vs. the average velocity of nitrogen.

As shown in the figure, the permeance is a function of the flow rate (velocity of the flow) in the lumen. This indicates that, in the nitrogen-purging method, the mass-transfer resistance is controlled by the diffusion in the gas boundary layer adjacent to the membrane in the lumen. Therefore, the

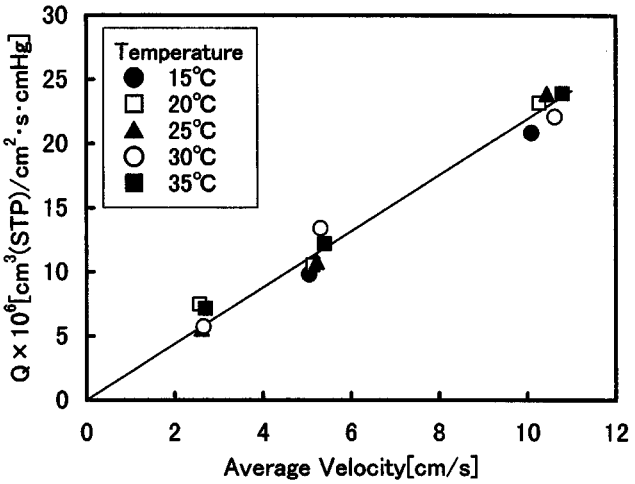

Figure 10. Permeance of water vapor vs. average velocity in nitrogen-purging method.

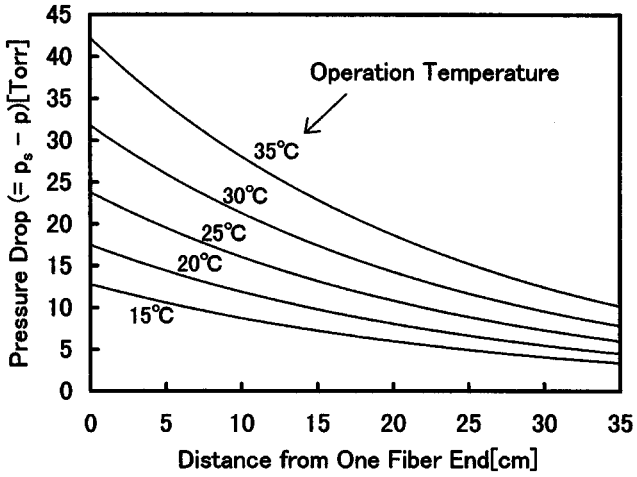

Figure 11. Calculated pressure drop profiles in the lumen in nitrogen-purging method.

overall permeance of water vapor, Q, can be given by

$$\frac{1}{Q} = \frac{1}{Q_m} + \text{function}(\bar{u}), \tag{17}$$

where Q_m is the permeance of water vapor in the membrane. It is considered to be equivalent to the permeance calculated through the experiments in the internal-flow module.

Figure 11 contains the partial pressure drop profiles of water vapor in the lumen. We can use these results (in Figures 10 and 11) to emphasize that the analysis of the permeance, in addition to those of the pressure and the velocity profiles for the flow in the lumen, is important. In other words, the permeance of water vapor is not a constant and must be a function of the flow through the lumen. Although the results obtained here should not be applied for vacuum degassing directly, they gave us an insight that was helpful in developing the modified theoretical model for vacuum degassing.

Modified theoretical analysis for vacuum degassing

From the preceding analytical results of the nitrogen-purging method, it was found that the diffusivity in the lumen might not be negligible. This can be applied to vacuum degassing. Needless to say, however, there are no elements except water vapor in vacuum degassing. Therefore, the diffusion mechanism in the vacuum condition with a single element is different from that of the nitrogen-purging method. The Hertz–Knudsen equation is generally used for analysis of diffusion in the vacuum condition. This equation can be applied for the static condition, in which no flow exists. On the other hand, in our study there is a flow in the lumen. As mentioned earlier, the velocity decreases and finally approaches zero when the distance from one fiber end increases. So we thought that the Hertz–Knudsen equation could be used to analyze the diffusion at the point at which water vapor flow became very low. If the equation is applied for the transfer in the lumen, the diffusion flux can be affected by the rate of flows along the lumen. In other words, the flux that diffuses vertically from the membrane wall should be a function of the flow rate (that is, the velocity in the lumen). So, we assumed that the overall permeance of water vapor, which consisted of the permeance of the membrane and the diffusion in the lumen, was a function of velocity in the lumen, just as in the nitrogen-purging method. Although the relationship between the permeance and the velocity is unknown, we assumed that Eq. 17 could be used for vacuum degassing.

If this assumption is correct, the theoretical model for vacuum degassing must be modified. However, the relationship between the permeance and the velocity are not known.

Here, for the relationship, we assumed the following:

$$\frac{1}{Q} = \frac{1}{Q_m} + \frac{1}{\alpha \times \bar{u}^{\beta}}, \tag{18}$$

where α and β are the parameters for the analysis. Generally speaking, those parameters have to be determined through experiments. But in our study, this approach was almost impossible because the velocity in the lumen was assumed to be a function of the distance (see Figure 8). Those parameters were therefore examined by comparing the experimental results of the transfer rate of water vapor (that were shown in Figures 2 and 3) and the analytical results using the estimated values of α and β. Here, $\alpha = \infty$, 1×10^{-6}, 5×10^{-6}, and $\beta = 1$ were employed. We examined β in the range from 0.5 to 2.0. As a result, it was found that $\beta = 1$ was suitable for our study.

Finally, as shown in Figures 12a and 12b, we obtained modified analytical results by calculating the governing equations shown in Eqs. 7, 11, and the relationship shown in Eq. 18.

Figures 12a and 12b show the pressure profiles and the velocity profiles, respectively. In this figure, the solid lines

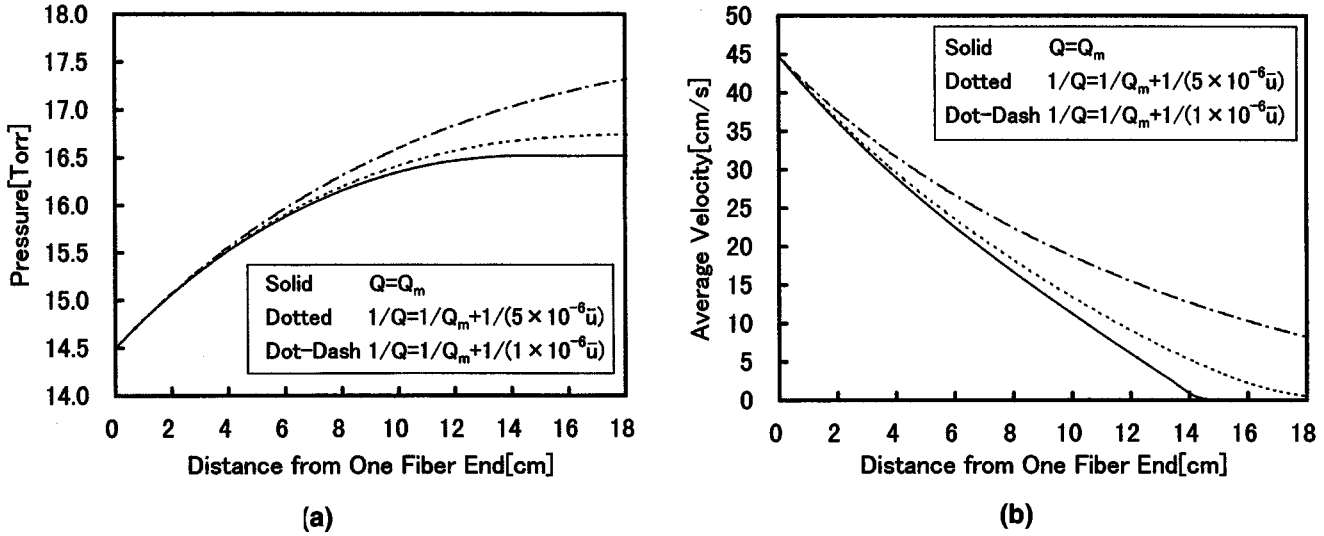

Figure 12. (a) Calculated profiles in the lumen on vacuum degassing: (a) pressure; (b) velocity.

Conditions for calculation: temperature: 25°C; pressure at one fiber end: 14.5 torr; transfer rate of water vapor: 8.7 mol/h.

correspond to the $\alpha = \infty$ and $\beta = 1$ condition, the dotted and dot-dash lines are for $\alpha = 5 \times 10^{-6}$, $\beta = 1$, and $\alpha = 1 \times 10^{-6}$, $\beta = 1$, respectively.

As shown in the figure, the parameters influence the pressure and velocity profiles. Especially as indicated in Figure 12b, when $\alpha = 1 \times 10^{-6}$, $\beta = 1$, or $\alpha = 5 \times 10^{-6}$, $\beta = 1$ in Eq. 18 is adopted, the flow exists at positions farther away from one fiber end compared to the condition of $\alpha = \infty$ and $\beta = 1$. Also the average velocity gradually becomes slower as the flow moves away from that end. These results suggest that, as the length of the hollow fibers becomes longer, the gases permeating through the membrane are not removed efficiently by the external-flow modules.

To confirm these results, it is necessary to analyze the mass transfer of oxygen in the lumen. The results given in this article showed, however, that fibers that are too long cause loss of efficiency for the external-flow modules.

Figure 13 shows the velocity profiles under different conditions for operation pressure. Here, in Eq. 18, $\alpha = 5 \times 10^{-6}$ and $\beta = 1$ are employed. As shown in this figure, the velocity gradients decrease as the operation pressure increases. This figure indicates that the operation pressure exerts a significant influence on the velocity profiles.

Similarly, Figure 14 gives the influence of operation temperature on velocity profiles. This figure shows that the velocity in the lumen increases with the temperature increase.

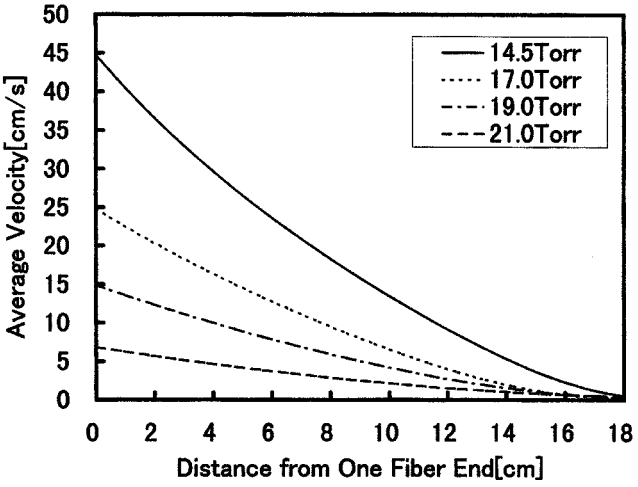

Figure 13. Effect of operation pressure on velocity profiles.

Conditions for calculation: temperature: 25°C; water flow rate: 1000 L/h; $\alpha = 5 \times 10^{-6}$, $\beta = 1$ in Eq. 18.

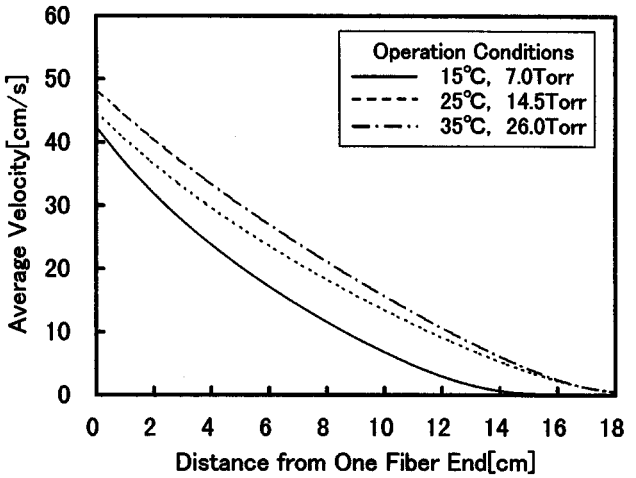

Figure 14. Effect of operation temperature on velocity profiles.

Conditions for calculations: temperature: 25°C; water flow rate: 1000 L/h; $\alpha = 5 \times 10^{-6}$, $\beta = 1$ in Eq. 18.

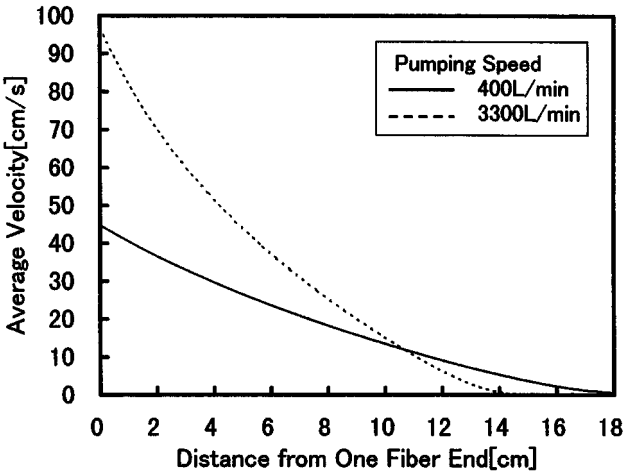

Figure 15. Effect of pumping speed of vacuum pump on velocity profiles.

Conditions for calculation: temperature: 25°C; water flow rate: 1,000 L/h; $\alpha = 5\times10^{-6}$, $\beta = 1$ in Eq. 18.

Also, as the temperature increases, the flow exists at a deeper point in the lumen. Therefore, we can say that the higher operation temperature contributes to the efficiency of the module's performance.

Table 2. Experimental Data vs. Calculated Results for Transfer Rate of Water Vapor

Run No.	Pumping Speed [L/min]	Temp. [°C]	Pres. [torr]	Transfer Rate of Water Vapor [mol/h] Obs.	Calc.
1	400	15	7.0	4.12	4.11
2			9.0	2.47	2.46
3			11.0	0.66	0.64
4	400	20	10.0	5.50	5.48
6			12.0	3.17	3.15
7			14.0	1.61	1.59
8			15.5	0.46	0.44
9	400	25	14.5	8.70	8.65
10			17.0	5.65	5.63
11			19.0	3.79	3.74
12			21.0	1.92	1.83
13	400	30	18.5	11.68	11.65
14			21.0	9.49	9.46
15			23.0	7.07	7.04
16			25.0	4.96	4.93
17			27.0	2.87	2.83
18	400	35	26.0	16.29	16.24
19			28.0	13.99	13.93
20			30.0	11.33	11.28
21			33.0	7.19	7.15
22			36.0	4.35	4.28
23	3,300	25	9.0	11.66	11.64
24			12.5	8.15	8.13
25			15.0	5.97	5.95
26			17.0	4.14	4.12
27			20.0	1.37	1.34

*$\alpha = 5\times10^{-6}$ and $\beta = 1$ are employed in Eq. 18.

Figure 15 shows the effect of the pumping speed of the vacuum pumps used to degas the velocity profiles. As shown in this figure, the velocity gradients increase as the pumping speed increases. This figure implies that vacuum pumps that are too large are undesirable. These results are essential for the design and operation of degassing modules.

Table 2 contains comparisons of the experimental results and analytical values from the proposed theory. In this table, the pumping speed is that of the vacuum pumps. Two types of vacuum pumps, with pumping speeds of 400 L/min and 3300 L/min, were used in this study. The temperature and the pressure are the operation temperature and operation pressure, respectively.

The experimental data for the transfer rate of water vapor are shown as those observed, while the analytical values of the transfer rate can be calculated by the following relationship:

$$\text{Transfer rate of water vapor} = m\cdot\int_0^L Q(p_s - p)\cdot 2\pi R_{\text{in}}\, dz. \tag{19}$$

The preceding equation means that integration of the pressure profile multiplied by the permeance and the membrane area yields the water-vapor transfer rate. Here, we use Eq. 18, $\alpha = 5\times10^{-6}$, and $\beta = 1$, so that the calculated results agree with the experimental results for all operation conditions, as shown in this table. Therefore, we can say that the theory proposed in this study is appropriate for the analysis of water-vapor transport phenomena in the lumen.

Also, the theory proposed here can be applied to fibers of shorter or longer lengths and other kinds of membranes. The optimal length of the fibers can be found for designing high-performance degassing modules, especially for vacuum degassing. These results are useful for the design of degassing modules.

Conclusions

Transfer mechanisms for water vapor in degassing modules were studied by using experiments of the vapor transfer rate and theoretical analysis of the pressure and velocity profiles in the lumen. In this article, we indicated that an understanding of the flow in the lumen is very important for the design and operation of degassing modules. The length of the hollow fibers also must be considered in developing larger modules for industrial-level operations.

In this study, we ignored the permeation flux through the membrane wall and assumed the velocity profile in the lumen to be parabolic. From the analyses, it was found that the permeation flux constituted less than a few percent of the axial flux. This means that the permeation flux has little influence on the velocity profile in the lumen. We can therefore say that this assumption is acceptable.

In developing a modified theoretical model for vacuum degassing, the diffusion term was introduced into the overall permeation in the lumen. We think that this modified model is more accurate than the first model, but further studies are

needed to understand the water-vapor transfer mechanism in the lumen.

The results obtained here are the first step in establishing a design strategy for highly efficient external-flow degassing modules. More detailed studies that consider dissolved oxygen and nitrogen transfer in the lumen are now required. Here, the flow of the treated water on the shell side plays a dominant role in the transfer of oxygen and nitrogen. Therefore, the strict analyses of the degassing modules require an understanding of both the lumen-side and shell-side flows of these gases.

In this article, we have discussed the mechanism of water-vapor transfer in the degassing modules. Our methods can be applied to other gas–liquid contactors.

Notation

M_r = parameter in Eq. 9
R = gas constant, J/mol·K
R_{out} = outer fiber radius, m
T = temperature, K
$u(r)$ = velocity of gas inside the hollow fiber, m/s

Greek letters

Ω_v = parameter in Eq. 9
σ = parameter in Eq. 9

Literature Cited

Bessarabov, D. G., E. P. Jacobs, R. D. Sanderson, and I. N. Beckman, "Use of Non-Porous Polymeric Flat-Sheet Gas-Separation Membranes in a Membrane-Liquid Contactor: Experimental Studies," *J. Memb. Sci.*, **113**, 275 (1996).

Federspiel, W. J., J. L. Williams, and B. G. Hattler, "Gas Flow Dynamics in Hollow-Fiber Membranes," *AIChE J.*, **42**, 2094 (1996).

Lemanski, J., and G. G. Lipscomb, "Effect of Shell-Side Flows on Hollow-Fiber Membrane Device Performance," *AIChE J.*, **41**, 2322 (1995).

Li, K., I. Chua, W. J. Ng, and W. K. Teo, "Removal of Dissolved Oxygen in Ultrapure Water Production Using a Membrane Reactor," *Chem. Eng. Sci.*, **50**, 3547 (1995).

Wang, K. L., and E. L. Cussler, "Baffled Membrane Modules Made with Hollow Fiber Fabric," *J. Memb. Sci.*, **85**, 265 (1993).

Yang, M. C., and E. L. Cussler, "Designing Hollow Fiber Contactors," *AIChE J.*, **32**, 1910 (1986).

Manuscript received May 4, 1998, and revision received Sept. 28, 1998.